amount. Since $\mathbf{X}^*$ corresponds to a local minimum of function $V(\mathbf{X})$ we have $V(\mathbf{X}_0) > V(\mathbf{X}^*)$ and, as a consequence, the system enters the tunnelling phase: as long as $V(\mathbf{X})$ is higher than V^* the state of the system moves away from $\mathbf{X}^*$. When it reaches a point for which $V(\mathbf{X})$ is less than V^* the system enters the gradient descent phase and stabilises to a different equilibrium point. To enable other (lower $V(\mathbf{X})$ energy) memories to be visited, the last local minimum becomes $\mathbf{X}^*$, the new initial state is again a slightly peturbed version of it, and the process reenters the tunnelling phase. Eventually, the system state rests on the lowest energy equilibrium.

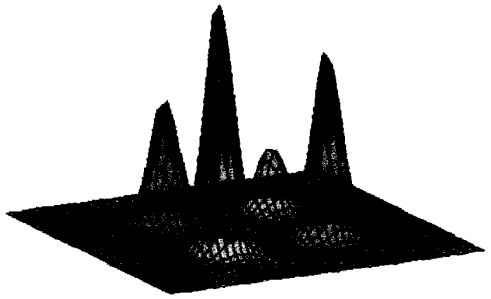

Fig. 1 *Lyapunov function as defined in eqn. 2, with N = 2 and M = 4*

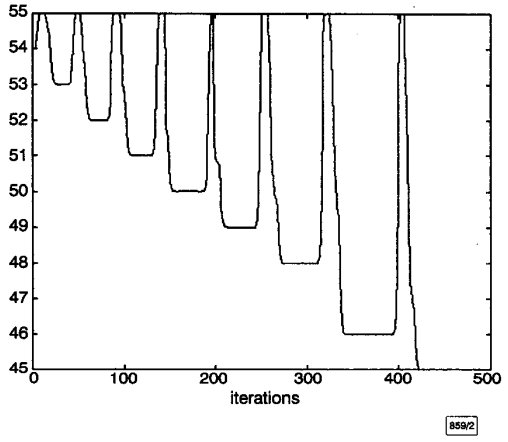

Fig. 2 *Typical evolution of combined energy function of system of eqn. 4*

Note that if the stored memories are to be visited in a predefined order, the weights vector $\{w_m\}$ should be carefully readjusted at the transition between the gradient descent and the tunnelling phase, to ensure that the next equilibrium to be reached has a lower energy than the preceding one. Moreover, in a multidimensional space ($N > 1$) a successful search is not always guaranteed. Typically, multiple runs starting from different initial conditions must be performed in order to realise the desired memory.

We have tested the proposed approach on a memory storing the 0–9 digits. The data were represented as 6×6 pixels: black pixels were coded as 1s and white pixels as 0s. The order of the dynamic system implementing the memory is $N = 36$, $\sigma_m = 0.5$, $\alpha = 0.5$. The weight vector was: $\{w_m\} = \{1, 2, 3, 4, 5, 6, 7, 8, 9, 10\}$ in order to force the stored memories to be visited in ascending order. In Fig. 2 we present a typical evolution of the combined energy function of the system, which includes both function $V(\mathbf{X})$ and the contribution of the repelling term. The system successively passes through all the stored equilibria.

10 March 1999

Electronics Letters Online No: 19990544

DOI: 10.1049/el:19990544

I.B. Ciocoiu (*Technical University Iasi, Faculty of Electronics and Telecommunications, PO Box 877, Iasi, 6600, Romania*)

E-mail: iciocoiu@etc.tuiasi.ro

References

1 HIRSCH, M.W., and SMALE, S.: 'Differential equations, dynamical systems and linear algebra' (Academic, New York, 1974)

2 HAN, J.Y., SAYEH, M.R., and ZHANG, J.: 'Convergence and limit points of neural networks and its application to pattern recognition', *IEEE Trans.*, 1989, **SMC-15**, (5), pp. 1217–1222

3 CIOCOIU, I.B.: 'Analog decoding using a gradient-type neural network', *IEEE Trans.*, 1996, **NN-7**, (4), pp. 1034–1038

4 BARHEN, J., PROTOPOPESCU, V., and REISTER, D.: 'TRUST: A deterministic algorithm for global optimization', *Science*, 1997, **276**, (5), pp. 1094–1097

Neural network based electronic nose for apple ripeness determination

E.L. Hines, E. Llobet and J.W. Gardner

It is possible to non-destructively determine apple ripeness using a simple electronic nose. The instrument employs tin oxide resistive gas sensors and neural networks (fuzzy ARTMAP, LVQ and MLP) to classify the samples into three states of ripeness with 100% accuracy. Fuzzy ARTMAP was found to be the best classifier in the presence of simulated Gaussian noise.

Introduction: One of the main concerns of the fruit industry is the systematic determination of fruit ripeness, because variability in ripeness is perceived by consumers to represent a lack of quality. The traditional methods used to assess fruit ripeness are destructive and thus cannot be systematically applied. These rely on the measurement of fruit firmness (penetromy), or chemicals related to ripeness such as pH, acidity (titration), soluble solids (refractometry), or ethylene (chromatography) [1]. More recently, non-destructive methods such as nuclear magnetic resonance (NMR) [2], proton magnetic resonance (PMR) [3], vision systems (skin colour) [4] and acoustic methods [5], have been proposed. However, NMR and PMR generally require expensive equipment. Acoustic methods involve the problem of how to couple the acoustic impedances of the emitter and the fruit; and also the fruit colour is in some cases only weakly correlated to ripeness. Another non-destructive strategy consists in sensing the aromatic volatiles emitted by the fruit using electronic noses [6]. Electronic noses are based on inexpensive, solid-state sensors, which are sensitive to ethylene (the ripening hormone in climacteric fruit, namely apples) and to other volatile compounds emitted by fruit. The sensor signals are processed by a pattern recognition engine (PARC). Neural networks (basically the MLP) have been extensively used for the PARC, and good results have been reported in the classification of foodstuffs [7]. However, it has been shown [8] that, in some cases, the fuzzy ARTMAP and LVQ paradigms outperform the MLP in aroma analysis.

In this Letter we demonstrate that an electronic nose, employing an array of only four sensors, in combination with neural networks, can accurately classify the ripeness of apples.

Experimental procedure: A set of apples (golden delicious) were put into a standard plastic food vessel (5l). An identical but empty plastic vessel was used as a reference. The vessels had two small holes in their cover, to allow the headspace to be analysed with the electronic nose. The sensor system comprised four commercial tin oxide gas sensors (TGS 822, 824, 825 and 881) from Figaro Engineering Inc., Japan. One measurement comprised taking alternatively a sample of the headspace of the apple vessel (10 min) followed by the reference vessel (50min). Measurements were gathered over a period of 21 days.

Results: (i) *Category establishment*: The choice of the data preprocessing algorithm has been shown to affect the performance of the pattern recognition stage. In this case a difference model (i.e. static change in sensor resistance) $\Delta R = R^{air} - R^{odour}$ and a differential model $\Delta R/R_0 = (R^{air} - R^{odour})/R^{air}$ were used.

Different classification methods such as PCA and fuzzy c-means clustering (FCM) were applied to verify that the categories established by each method were not arbitrary (i.e. were consistent with

the state of ripeness). The use of differential pre-processing led to the best separation between categories with PCA (see Fig. 1). The data were mean-centred prior to the analysis. In this case the two first principal components were kept (94% of variance in data). Three different categories were established. Category *a* (green apples) clusters measurements performed during the first two days (16 samples). Category *b* (green with some yellow) comprises measurements performed during days 3 – 9 (37 samples). Category *c* (yellow) groups measurements from the 10th to 21st day (97 samples). From left to right in Fig. 1, categories *a*, *b* and *c* appear to be ordered according to increasing fruit ripeness. The cluster corresponding to category *a* shows a significant spread. This is because this category corresponds to green apples, which emit volatiles at very low concentration.

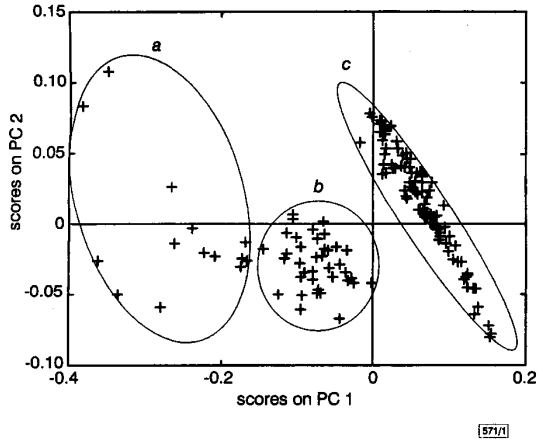

Fig. 1 *Results of PCA*

Measurements cluster in three categories (*a*, *b* and *c*) of fruit ripeness

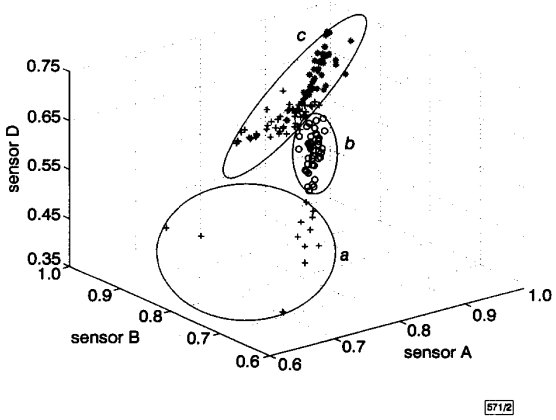

Fig. 2 *Results of FCM*

Clusters represent three different categories of state of ripeness

Fuzzy *c*-means (FCM) (differential pre-processing) was applied (see Fig. 2). Categories *a*, *b* in FCM were consistent with categories *a* and *b* in PCA. Category *c* in PCA was split into two clusters in the FCM results. However, it can be concluded that both methods led to very similar results, which were consistent with the peel colour. Therefore, the three categories established by PCA were used as the basis on which to apply supervised neural network classifiers.

(ii) *Neural networks*: The datasets were analysed using the fuzzy ARTMAP, LVQ and the back-propagation trained MLP paradigms. Fuzzy ARTMAP and LVQ carry out supervised learning, as does the back-propagation MLP. But unlike back-propagation, fuzzy ARTMAP and LVQ are self-organising and self-stabilising. For this analysis, the data were split into four folds. While two folds consisted of 112 training vectors and 38 test vectors, the other two consisted of 113 training vectors and 37 test vectors. Test vectors were selected at random without replacement. Since the number of vectors per category was uneven (e.g. 97 replicates in category *c* and 16 replicates in category *a*), each category was represented in both training and testing sets in proportion to its number of replicates. The networks used had four inputs (one per sensor in the array) and three outputs (since a 1-of-3 code was used to code the three different states of ripeness). MLP had four nodes in the hidden layer, LVQ had 15 nodes in the competitive layer and fuzzy ARTMAP had six nodes committed after training. Table 1 summarises the results for the different networks studied. The performances of the three networks were similar but the time necessary to train the networks was very different. While fuzzy ARTMAP required only 100 cycles, LVQ and MLP required 1500 and 20000 epochs, respectively.

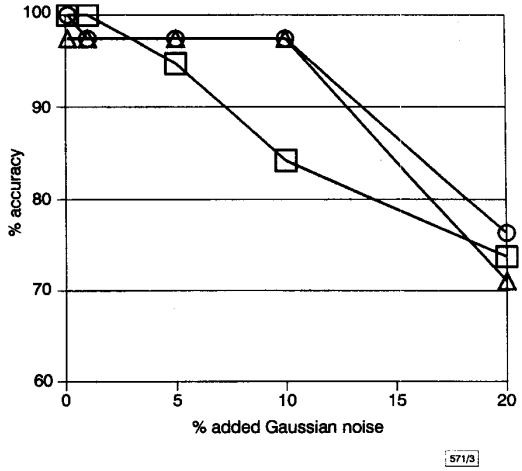

Fig. 3 *Accuracy in classification of state of ripeness of apples reached by fuzzy ARTMAP, LVQ and MLP in presence of 0, 5, 10 and 20% of added Gaussian noise*

○ fuzzy ARTMAP
□ LVQ
△ MLP

Table 1: State of ripeness classification with fuzzy ARTMAP, LVQ and MLP

Method	Fold 1	Fold 2	Fold 3	Fold 4	Overall
Fuzzy ARTMAP	38 (38)	38 (38)	37 (37)	37 (37)	150 (150)
LVQ	38 (38)	38 (38)	37 (37)	37 (37)	150 (150)
MLP	38 (38)	38 (38)	37 (37)	37 (37)	146 (150)

Patterns correctly classified (patterns to be classified)

(iii) *Noise rejection*: To analyse how the different networks were able to deal with uncertainty, which is a key factor in any measurement system, different levels of Gaussian noise (5, 10 and 20%) were added to the sensor responses and the classification process was repeated. Fig. 3 shows the results. For this application, the performances of fuzzy ARTMAP and the MLP were more resilient to low values of noise (up to 10%) than the performance of LVQ.

Conclusions: The usefulness of electronic nose instruments to non-destructively assess the state of ripeness of apples has been demonstrated. Fuzzy ARTMAP, LVQ and MLP neural networks were applied to the classification of the state of ripeness of apples. An accuracy of 100% was obtained for fuzzy ARTMAP and LVQ. The training time of fuzzy ARTMAP was found to be typically more than an order of magnitude faster than back-propagation MLP and LVQ. Furthermore, fuzzy ARTMAP was shown to perform better than LVQ in the presence of Gaussian noise.

Acknowledgments: E. Llobet acknowledges financial support (PR1997-0138) from the Spanish MEC during his stay at Warwick University.

22 February 1999
Electronics Letters Online No: 19990547
DOI: 10.1049/el:19990547

E.L. Hines and J.W. Gardner (*Division of Electrical and Electronic Engineering, School of Engineering, Warwick University, Coventry CV4 7AL, United Kingdom*)

E. Llobet (*Department of Electronic Engineering, Universitat Rovira i Virgili, Autovia de Salou s/n, 43006 Tarragona, Spain*)

References

1 PARE, J.R.J., and BELENGER, J.M.R. (Eds.): 'Instrumental techniques in food analysis' (Elsevier, Amsterdam, 1997)
2 CHO, S.I., KRUTZ, G.W., GIBSON, H.G., and HAGHIGHI, K.: 'Magnet console design of an NMR-based sensor to detect ripeness of fruit', *Trans. ASAE,* 1990, **33**, (4), pp. 1043–1050
3 WAI, W.K., STROSHINE, R.L., and KRUTZ, G.W.: 'Modified Hahn echo pulse sequence for proton magnetic resonance (1H-MR) measurements of percent soluble solids of fruits', *Trans. ASAE,* 1995, **38**, (3), pp. 849–855
4 WARD, G., and NUSSINOVITCH, A.: 'Peel gloss as a potential indicator of banana ripeness', *Lebensm.-Wiss. u.-Technol.,* 1996, **29**, pp. 289–294
5 GALILI, N., SHMULEVICH, I., and BENICHOU, N.: 'Acoustic testing of avocado for fruit ripeness evaluation', *Trans. ASAE,* 1998, **41**, (2), pp. 399–407
6 SIMON, J.E., HETZRONI, A., BORDELON, B., MILES, G.E., and CHARLES, D.J.: 'Electronic sensing of aromatic volatiles for quality sorting of blueberries', *J. Food Sci.,* 1996, **61**, (5), pp. 967–970
7 GARDNER, J.W., and BARTLETT, P.N.: 'Electronic noses: Principles and applications' (Oxford University Press, 1999)
8 LLOBET, E., HINES, E.L., GARDNER, J.W., BARTLETT, P.N., and MOTTRAM, T.T.: 'Fuzzy ARTMAP based electronic nose data analysis', submitted to *Sens. Actuators B,* 1999,

1000km transmission of 40Gbit/s single channel RZ data over dispersion managed standard (non-dispersion shifted) fibre

S.B. Alleston, P. Harper, I.S. Penketh, I. Bennion, N.J. Doran and A.D. Ellis

Error-free transmission of a single polarisation optical time division multiplexed 40Gbit/s dispersion managed pulse data stream over 1009km has been achieved in dispersion-compensated standard (non-dispersion shifted) fibre. This distance is twice the previous record at this data rate.

Introduction: There is much interest at present in techniques for upgrading existing terrestrial standard fibre transmission lines through the use of novel modulation formats and dispersion management [1]. We have recently reported preliminary transmission results at 40Gbit/s over 509km of standard fibre using a simple dispersion compensation technique [2]. This compared favourably with alternative methods including polarisation multiplexing [3] and mid-span spectral inversion that acheived a 400 km propagation distance at the same data rate [4, 5]. However, numerical simulations have suggested that the adoption of a modified dispersion compensation format should extend the achievable 40Gbit/s transmission distance to > 2000km of standard fibre [6]. We now report the experimental achievement of error-free propagation of a single polarisation 40Gbit/s RZ data stream over a transmission distance of 1000km in standard fibre, representing the first demonstration of 40Gbit/s transmission in standard fibre over this distance and exceeding our previous achievement by a factor of 2. These results were obtained using a single length of dispersion compensating fibre in each amplifier span, and imply the realistic prospect of upgrading standard fibre systems to 40Gbit/s by a straightforward passive scheme.

Experiment: The experimental setup is shown in Fig. 1. The jitter supressed gain switched DFB source provided 7.2ps pulses with a time-bandwidth product of 0.45 at the operating wavelength of 1557nm. A 10Gbit/s 2^{31}–1 PRBS data pattern was imposed on the ECMLL pulse stream by a lithium niobate amplitude modulator (AM), and this bit stream was multiplexed up to 40Gbit/s using a fibre delay line multiplexer (MUX) in a now standard configuration. The transmission experiments were carried out using a single span recirculating loop containing a single erbium doped fibre amplifier (EDFA) and a 2.3nm optical bandpass filter. The loop itself consisted of 32.3km of standard fibre (SF), in section lengths of 14.2km before and 18.1km after the EDFA respectively, with an average dispersion of +16ps/(nm km) and 6.8km of dispersion compensating fibre (DCF) with a dispersion of –76ps/(nm km). The average dispersion zero wavelength was 1556nm and at the operating wavelength the overall average dispersion was +0.03ps/(nm km), the DCF also providing partial slope compensation resulting in a value of +0.03ps/(nm² km) for the fibre combination.

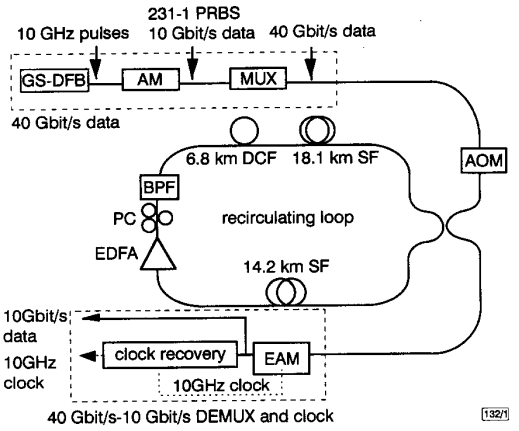

Fig. 1 *Schematic diagram of experimental setup showing the 40Gbit/s data generator, recirculating loop and 40Gbit/s to 10Gbit/s demultiplexer*

Results: The 40Gbit/s data stream was demultiplexed to 10Gbit/s using an electroabsorbtion modulator (EAM) and a following 10GHz phase locked loop (PLL) clock recovery unit [7]. The recovered clock was used as a trigger for both the bit error rate and sampling oscilloscope measurements, and to drive the EAM.

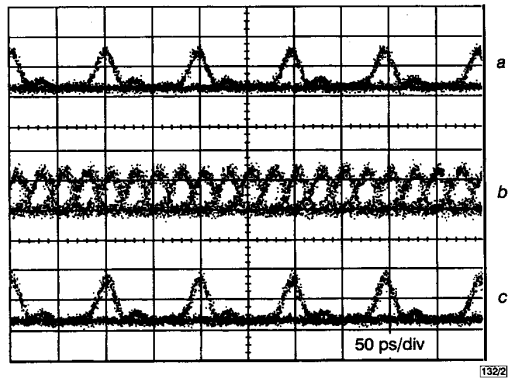

Fig. 2 *Eye diagrams for 10Gbit/s back-to-back performance, 40Gbit/s multiplexed data and demultiplexed 10Gbit/s data*

a 10 Gbit/s, back-to-back
b 40 Gbit/s, multiplexed
c 10 Gbit/s demultiplexed

Separate 10Gbit/s channels were selected by means of a microwave phase shifter (PS) connected to the EAM drive line. Fig. 2 shows eye diagrams corresponding to *a* the 10Gbit/s back-to-back performance, *b* the multiplexed 40Gbit/s data stream, and *c* the demultiplexed 10Gbit/s channel, respectively, indicating little signal degradation after demultiplexing. Identification of the correct location of the data insertion/extraction point in the fibre span represents a crucial aspect of these experiments. The high values of local dispersion and the relatively narrow pulse width employed combine to produce a large map strength [8] of 25, highlighting a significant issue for 40Gbit/s dispersion managed standard fibre